AN IMPROVED INSIGHT INTO LOW-SALINITY WATERFLOODING: IN-SITU CHARACTERIZATION OF WETTABILITY ALTERATION AT ELEVATED PRESSURE AND TEMPERATURE CONDITIONS

M. Khishvand, A.H. Alizadeh, I. Oraki Kohshour, M. Piri
Department of Petroleum Engineering, University of Wyoming, Laramie, WY 82071, USA
This paper was prepared for presentation at the International Symposium of the Society of Core Analysts held in Snowmass, Colorado, USA, 21-26 August 2016

ABSTRACT
Low-salinity waterflooding (LSWF) is known as one of the most effective improved oil recovery techniques that could result in significant additional recovery compared to conventional high-salinity waterflooding (HSWF). Although numerous laboratory studies have confirmed the effectiveness of LSWF under specific conditions, they have mostly failed to present explicit evidences on the pore-level mechanisms that are responsible for the observed improvement in recovery. In this study, we investigated LSWF production mechanisms using X-ray micro-computed tomography (micro-CT) and examined recovery trends at the pore scale. Two core-flooding experiments were performed on miniature reservoir sandstone core samples at elevated pressure and temperature conditions. The preserved core samples (5 mm in diameter) were cut and then saturated to establish reservoir initial saturation conditions. The samples were subsequently waterflooded with low- and high-salinity brines and imaged using a micro-CT scanner. Micro-CT images were then used to obtain fluid saturations and three-dimensional maps of fluid occupancy during each experiment. High-resolution micro-CT images were also analyzed to measure pore-scale contact angles and study in-situ wettability and its impact on oil mobilization during different stages of waterflooding process.

The results highlight a significantly improved performance in LSWF compared to that of HSWF. The LSWF test showed more prolonged oil recovery response and gradual recovery at later stages while the HSWF recovery stabilized much earlier. Pore-scale contact angle measurements yielded direct evidence of wettability alteration from weakly oil-wet toward weakly water-wet conditions during LSWF; however, no considerable changes were observed in in-situ contact angles during the HSWF. Investigation of fluid occupancy maps along with in-situ characterization of wettability allowed us to establish a significantly better understanding of pore-scale mechanisms responsible for improved recover by LSWF.

INTRODUCTION
Waterflooding has been frequently implemented as an improved oil recovery (IOR) method to maintain reservoir pressure and sweep oil toward production wells. This technique was first practiced in 1880 [1] and since then has been adopted as one of the

most widespread methods for oil recovery. Due to the success of this IOR scheme in numerous oilfields, a large number of studies have targeted different aspects of waterflooding. Yildiz and Morrow [2] found that reservoir wettability and composition of injected and connate brines considerably affect waterflood recovery. These findings immediately inspired scientists to focus on composition and salinity of injected brine as the only controllable parameters to obtain higher waterflood efficiency. Primary research on outcrop Berea sandstone samples revealed that reducing salinity of the injected brine had a substantial effect on the amount of trapped oil saturation [3 and 4]. This method, so called low-salinity water flooding (LSWF), soon became one of the most promising IOR techniques. It was observed that LSWF resulted in remarkably higher recoveries in both sandstone [5] and carbonate [6] rock samples. In some cases, single well tracer tests [8] proved the favorable laboratory results. LSWF can be performed under secondary mode (at initial water saturation) or tertiary mode (at waterflood residual oil saturation). Either way, it may offer notably higher recovery efficiency compared to high-salinity waterflooding (HSWF). During the last decade, numerous laboratory tests have been conducted to evaluate the effectiveness of LSWF, investigate conditions under which LSWF succeeds, and describe displacement mechanisms governing LSWF recovery. The observations have demonstrated that the success of LSWF is greatly influenced by the original reservoir wettability and fluids present in the pore space (i.e., connate brine and crude oil). Tang and Morrow [3] reported three conditions that are necessary, but not sufficient, to observe low-salinity effect (LSE). These include significant clay content, presence of connate water, and exposure to crude oil to make a mixed-wet condition. Although some studies have shown the LSE for clay-free sandstone [9] and carbonate samples [7], these three conditions are universally pervasive to select candidate reservoirs for LSWF.

To perform successful LSWF, the underlying displacement mechanisms responsible for LSE must be comprehensively understood. Over the years, many research studies have been devoted to probe physical phenomena and displacement mechanisms that explain the higher recovery of LSWF and enrich the fundamental understanding of the LSE; but still, no consistent and systematic answers have been presented [3]. Results of core-flooding experiments, such as saturation trends, effluents analysis, and pressure drop data have been used to provide some indirect evidences supporting mechanisms of the LSWF process. Most of these studies have discussed several main hypotheses supporting the observed increases in recovery during LSWF. The most well-known mechanisms are detachment and migration of mixed-wet clay fines [2] and associate wettability alteration [3, 10, and 11], multicomponent ion exchange (MIE) between the low-salinity brine (LSB) and clay surfaces [4 and 12], mineral dissolution [13], and saponification [7]. Among these, wettability alteration (due to limited release of mixed-wet clay fines and/or MIE) from mixed-wet toward increased water-wetness is one of the most supported and frequently suggested mechanisms. When an oil-wet rock surface is exposed to LSB, water destabilizes the clays, acts as a wettability modifier, and changes the wettability toward increased water-wetness. This indeed allows oil to be displaced from the oil-wet pores [11]. Although there have been some attempts based on pore-scale theoretical

models to explain the pore-scale subtleties of this phenomenon [11], no rigorous pore-scale experimental observations have been presented in this regard, and hence pore-scale explanation of displacement mechanisms that govern higher recovery of the LSWF remain as a question that has yet to be answered.

For years, scientists have performed macro-scale tests to probe the above-mentioned mechanisms, but have not been able to directly observe the rock-fluid interactions, such as wettability alteration, and dynamic reactive interplays occurring at the pore scale. This, perhaps is the most significant shortcoming of those studies. Recently, however, image-based techniques such as micro-computed tomography (micro-CT) imaging has been employed to eliminate the drawbacks associated with macro-scale tests. Micro-CT imaging is a technology by which a rock sample is imaged to map its internal morphology and pore-scale fluid occupancy during different flow processes [14-16]. Using this new technology, one can look inside the pore space during LSWF, monitor potential changes in wettability and saturation trends, and obtain direct observations of governing mechanisms for the LSE. A few research groups have attempted to take advantage of microtomography along with scanning electron microscope (SEM) imaging technique to observe mineral dissolution and fines migration during LSWF [9 and 13] and some successes have been achieved. However, due to technical difficulties and limitations of experimental procedures used, microtomography has not been used to investigate potential in-situ wettability alteration and its associated displacement events as, perhaps, the most important mechanism responsible for LSE.

In this work, we endeavoured to exploit micro-scale images generated during LSWF experiments to investigate wettability alteration and provide observational clues tying the in-situ wettability with governing displacement mechanisms. An extensive laboratory study was deployed on reservoir sandstone samples and using reservoir crude oil at reservoir conditions. We assembled a unique miniature core-flooding apparatus, which could be employed to perform experiments at reservoir conditions while the core holder is placed inside a micro-CT scanner and the sample is imaged in the course of the experiments. We carried out two sets of experiments (one HSWF and one LSWF) to first examine the efficiency of the LSWF compared to that of HSWF in reservoir sandstone samples, and secondly to investigate the potential wettability alteration during LSWF in order to develop a better understanding of the pore-scale displacement mechanisms responsible for LSE. We used an effective approach to directly measure in-situ contact angles in individual pores. In-situ wettability data along with spatial distribution maps of fluid phases were used to shed light on the displacement events responsible for LSE.

Experimental

In this section, we describe the rock samples and fluids used to perform the experiments. We then discuss the experimental setup utilized to conduct the tests followed by the experimental procedure.

Rock Samples

We performed the core-flooding experiments on nominally 5-mm diameter and 50-mm long miniature reservoir sandstone core samples labeled as Samples A and B. The samples were taken parallel to bedding from a 110-mm diameter preserved reservoir core sample. The parent core sample was loosely consolidated and extra effort was made to drill smooth miniature core samples. Air was used as a coolant to minimize disturbances to the samples. All samples were dry-cut, instantly placed into the core holder, and then undergone their corresponding experimental procedure. Additionally, a 25.4-mm core plug (Sample C) and an end trim (Sample D) were cut from the same parent core. Sample C was used to measure initial water saturation (S_{wi}) using dean-stark method. Dean-stark measurement showed S_{wi} of 13% for the preserved core after drilling. This sample was then solvent-cleaned and its porosity and permeability were measured. Sample D was used for XRD analysis that showed about 6% clay content, mainly kaolinite. The presence of connate water and the significant clay content suggested that this rock might be a good candidate for LSWF. For Samples A and B, porosity was measured using micro-CT images. Uniform porosity distributions (see Figure 1) verified the homogeneity of the samples. Geometrical and petrophysical properties of the rock samples are listed in Table 1.

Fluids

High-salinity brine (HSB) was synthetized using sea water formulation with a total dissolved solid (TDS) of 40,300 ppm. The synthetic brine was prepared by including most of the ions in order to replicate the sea water composition as closely as possible. This brine was then diluted with a ratio of one-fiftieth and utilized as the LSB. The oil phase was reservoir stock tank oil (i.e., dead crude oil). Crude oil was filtered through a 0.5-μm filter before use to remove residue and debris. We then added 6 vol. % diiodomethane as X-ray dopant to ensure sufficient contrast between the crude oil and aqueous solution in X-ray images. Since we used ethane in the course of the experiments, one could argue possible asphaltene precipitation when the crude oil came into contact with ethane. To investigate this, we mixed 10 cc of the crude oil with 50 cc of ethane in a high-pressure cell and frequently shacked the container at experimental conditions (i.e., 1000 psi and 60 °C) for a day. The fluid mixture was then removed and the precipitated asphaltene was measured. The test showed 0.29 wt.% of asphaltene precipitation, which was negligible and did not introduce any adverse uncertainties into the experiments. Density and viscosity of all fluids were either measured at experimental conditions or estimated from data available in the literature [18-20]. Fluid properties are summarized in Table 2.

Experimental Setup

We employed a unique experimental apparatus to carry out the micro-scale core-flooding tests at elevated pressure and temperature conditions. The core-flooding was integrated with a high-resolution micro-CT scanner to image the core samples in the course of the experiments. The experimental setup composed of four dual cylinder Quizix^{TM} pumps, a miniature core holder, a micro-CT scanner, Rosemount pressure transducers, and

appropriate heating systems. All wetted parts of the core-flooding system were made out of Hastelloy™, titanium, and other corrosion resistant material. Figure 2 exhibits a schematic diagram of the flow system used in this study. Pumps 1 and 2 withdrew brine and oil, respectively, from buckets, and injected them into the core samples. Fluids could be pressurized with their respective pumps and passed through controllable heat exchangers to reach desired temperatures prior to injection. Pump 3 received the effluents at desired constant pressures and kept the pore pressure stable. A net overburden pressure was maintained during all experiments using Pump 4. The custom-built core holder was fabricated from composite materials with minimum X-ray absorption. It had nozzles that directed the fluids from Pumps 1 and 2 into the core and from the core to the back pressure pump (i.e., Pump 3). A special heating system was coupled with the core holder and the flooding system to heat up the flooding vessels during the experiments. All lines were insulated to maintain the fluid temperature and minimize potential flow distortions due to the changes in the temperature. Further details of the core-flooding system can be found elsewhere [17].

Experimental Procedure

To conduct each experiment, the core sample was first cut and instantly loaded in the miniature core holder. A low (for easier access to the pore space) net confining pressure was applied. The sample was then flooded with ethane to remove bulk air from the pore space. The ethane flooding was performed at 100 psi back pressure and at moderately low gas flow rates to minimize the risk of vaporization of the connate brine. The sample was then scanned to capture a reference image. Afterward, pore pressure was reduced and the dead crude oil was introduced into the sample. When crude oil breakthrough and removed some of the bulk ethane, pore and net confining pressures were simultaneously increased to 800 and 900 psi, respectively. At this step, temperature of the system was gradually increased to 60 °C. These temperature and pressure conditions were fixed until the end of the experiment. The oil was allowed to remove ethane thoroughly with a miscible displacement process. Once the flow of oil was established, oil injection was continued for a day with a very low flow rate to ensure no ethane was left in the pore space. The core was frequently scanned for any evidence of hydrocarbon gas. When zero gas saturation was confirmed by the CT images, a scan was run to determine the initial water saturation profile along the sample. Thereafter, the core was flooded with desired brine at a pre-specified flow rate of 0.004 cc/min. The flow rate was equivalent to capillary numbers of 1.42E-07 and 1.48E-07 for LSWF and HSWF tests, respectively. Brine was injected with increments of 0.5 pore volume (at the outset of the experiment) and 1 pore volume (at the end). After each increment, we halted brine injection and the system was let come to rest. The middle section of the core sample, hereafter referred to as field of view (FOV), was then scanned. The final stage of each waterflood was achieved when the fluid occupancy no longer changed even by doubling the brine flow rate. Image sets were then reconstructed as form of stacked slices and prepared for analysis.

IMAGE ANALYSIS

The tomographic images obtained during the experiments were analyzed to map fluid occupancy and measure trapped oil saturation as well as fluid-rock properties. The image set captured at each stage of the experiments was segmented after registration with the reference image. The segmented data was used to characterize in-situ wettability by means of oil-brine contact angle measurement. This provided a platform to study the potential wettability alteration in the rock and the displacement mechanisms responsible for the LSWF recovery. A detailed explanation of the segmentation method and the procedure for contact angle measurements can be found elsewhere [14-16].

RESULTS AND DISCUSSION

In this section, we present the results of the micro-scale LSWF and HSWF experiments performed on Samples A and B. For each experiment, we used pore-scale fluid occupancy maps generated utilizing the micro-CT images to study displacement mechanisms and resulting saturation trends. This allowed us to highlight the efficiency of the LSWF compared to that of HSWF in the targeted rock samples. Furthermore, we characterized in-situ wettability at different stages of each flow process to probe potential wettability alteration during the LSWF. Finally, we attempted to connect the in-situ wettability alteration and its consequent pore-scale displacements with the saturation trends observed.

Pore-Scale Fluid Occupancy and Saturation

Figures 3 and 4 exhibit pore-scale fluid occupancy maps of the core samples subjected to the LSWF and HSWF, respectively. Each figure contains several images corresponding to different stages of each flow test and exemplifies the displacement events taking place in the pore space. As seen in Figures 3a and 4a, the pore space was dominantly occupied by oil before the commencement of the waterfloods. Oil almost entirely filled the large and medium-sized (mostly oil-wet) pores. Water, however, resided in very small (mostly water-wet) pores and crevices. This fluids arrangement established the initial mixed-wet conditions of the samples. As waterflooding initiated (Figures 3b for the LSWF and 4b for the HSWF), in both samples, water invaded into fully and partially oil-filled elements by two mechanisms. It displaced oil through imbibition from water-wet pores (with an order of smallest to largest) and upon drainage from oil-wet pores (with an order of largest to smallest). This could be realized when one compares Figures 3b and 4b with 3a and 4a. Water, initially, invaded into small water-wet pores (squares) and large oil-wet pores (circles) while medium-sized pores remained oil-filled. In other words, the oil clusters sitting in the medium-sized pores were the last ones to be mobilized by water. As waterflood proceeded (Figures 3c and 4c), water had more accessibility to the entrance of the oil-filled pores and hence, it invaded into a greater number of them including some medium-sized ones. Meanwhile, oil gets trapped in some pore elements depending on wettability and fluids present in the neighbouring elements. Finally, the waterfloods ended at a point that the remaining oil was entirely trapped (i.e., disconnected). This point, known as waterflood end point, signified the efficiency of the waterfloods. Comparison between Figures 3c and 3d and 4c and 4d revealed that the end point was

established after about 5 pore volumes of water injection (PVWI) for the HSWF; however, in the case of the LSWF, end point was obtained much later and pronounced changes in oil occupancy were observed even in late stages (until about 10 PVWI).

To determine the end points and examine the efficiency of the LSWF, saturation values were calculated over the FOVs for both waterfloods. The results are presented in Figure 5 for stages with the most considerable variations. Before waterflooding, initial oil saturations ($S_{oi} = 1 - S_{wi}$) were homogenous along the FOV and had very similar average values for both samples (about 0.91 and 0.90 for Samples A and B, respectively). These values were also consistent with the S_{oi} measured using dean-stark method for Sample C (i.e., 87%). After 5 PVWI, oil saturations were reduced in both samples with similar trends resulting in *remaining* oil saturations (S_{or}) of 0.46 and 0.45 for Samples A (LSWF) and B (HSWF), respectively. This in fact indicated similar initial recoveries of the LSWF and HSWF. Upon continuation of the waterfloods, for the HSWF, S_{or} stabilized and no further considerable oil production was observed, even with an increase in flow rate to 0.006 cc/min; therefore, this point was considered as wateflood residual oil saturation (S_{orw}) for the HSWF. In contrast, for the LSWF, S_{or} continued to reduce significantly at the later stages of waterflooding (until 10 PVWI) resulting in a S_{orw} of 0.30. These observations demonstrated that the LSWF had a considerable gradual recovery at later stages whereas the high-salinity production stabilized much earlier. These differences in recovery trends, known as LSE, are in line with our earlier observations of water-displacing-oil events in medium-sized pores occurred during the late stages of the LSWF (Figure 3d). We believe that when low-salinity brine contacted the rock surface, it changed the wettability toward increased water-wetness (see more details listed later in this section). The wettability alteration might be attributed to either migration of clay minerals or multiple ion exchange [3 and 5]. LSB gradually altered the wettability of the rock and as a consequence facilitated invasion of water into medium-sized oil-filled pores (see the rectangular area shown in Figure 3d). To verify this hypothesis, one would need to investigate whether wettability alteration does take place during the LSWF and how the potential alteration impacts oil displacement. In the next section, we explore this by means of in-situ wettability measurement and pore-scale investigation of displacement events motivated by potential wettability alteration.

In-Situ Characterization of Wettability Alteration

We accomplished a detailed analysis of the micro-scale images to find potential changes in wettability during different flooding scenarios. For each flooding step, the segmented data was analyzed to measure oil-water contact angles. The detailed methodology of the contact angle measurement can be found elsewhere [15 and 16]. We limited our measurements to contact angles at main terminal menisci (i.e., oil-water interfaces at the center of pore-throat junctions). Since we imaged the samples after the fluids were let to come to rest, contact angle measurements were considered to give equilibrium values. One should note that it was impractical to measure contact angles in very small (mainly water-wet) pores because the amount of oil present in those pores was extremely small. Contact angle measurement results presented in Figure 6 are for three stages of each

waterflood (i.e., after 0.5, 5, and 10 PVWI). Contact angle values show a distribution for each stage, which might be attributed to local mineral heterogeneity and microscopic surface roughness. As it can be observed, initial contact angle values (i.e., after 0.5 PV) showed similar distributions as well as mean values for the LSWF and HSWF. The average values of about 115 and 117 degrees for the LSWF and HSWF, respectively, verified a weakly oil-wet condition in the preserved samples. This figure also demonstrates that contact angles did not change during the course of HSWF, while substantial changes toward increased water-wetness occurred during the LSWF (from 115 to 89°). As the LSWF proceeded, LSB may have reacted with the clay minerals lining the rock surface. It has been hypothesized that LSB may detach the mixed-wet clay particles from the pore walls [3] and exchange divalent ions (such as Ca^{2+}) with the clays [5]. Both mechanisms may have contributed to the observed reduction in the oil-water contact angle. The bimodal graphs shown in Figure 6 (after 5 and 10 PV LSWF) indicate that contact angle could change significantly in some pores whereas others might show only slight alterations compared to their initial wettability condition. This might arise from several key factors such as different contact time and contact areas with the LSB as well as variable clay content of the pores.

Additional analysis of the pore-scale contact angles could further corroborate the displacement events that were discussed earlier as a consequence of wettability alteration during LSWF. Figure 7 depicts two-dimensional views of fluid occupancy in an individual pore and the corresponding measured contact angles after 0.5, 5, and 10 PVWI. This figure illustrates that water had access to the entrance of an oil-filled element in all stages, but interestingly, the pore was only invaded by water when the contact angle decreased. This can be explained by threshold capillary pressure concept [11]. Upon changes in wettability from 127 (after 0.5 PVWI) to 99 (after 5 PVWI), the threshold water pressure needed for the drainage process (i.e., water-displacing-oil in this oil-wet pore) was reduced, which in turn enabled water to proceed in the pore and displace the oil in the later stages (i.e., between 5 and 10PVWI). We believe that these changes in wettability and subsequent invasion of water into medium-sized oil-wet pores directed the gradual production of oil at late stages of the LSWF and were responsible for higher oil recovery of the LSWF. This study provided, for the first time, direct evidences of wettability alteration due to LSE and associated pore-scale mechanisms governing the greater recovery established by LSWF.

CONCLUDING REMARKS

In this study, we performed a LSWF and a HSWF micro-scale experiments on preserved reservoir sandstone core samples with reservoir fluids and at elevated pressure and temperature conditions. The preserved samples were cut and saturated using a special procedure to establish initial reservoir saturation. The samples were then flooded under secondary mode using brine with different salinities. We imaged the fluid occupancy in the pore space and used the images to characterize oil saturation and in-situ wettability as well as probing the physical mechanisms responsible for LSE.

The results indicated waterflood residual oil saturations (S_{orw}) of 0.30 and 0.45 for the LSWF and the HSWF, respectively. These observations highlighted the significant performance of LSWF compared to HSWF in our study. LSWF showed more prolonged oil recovery response (gradual recovery at later stages) while the HSWF recovery curve stabilized much earlier. Analysis of micro-CT images enabled us to measure pore-scale contact angles to examine wettability alteration of the rock surface. These measurements coupled with pore-scale fluid occupancy maps revealed that when the rock surface was exposed to low-salinity brine, the average oil-water contact angle gradually reduced toward neutral-wet condition (i.e., from 115 to 89), which in turn lowered the threshold water pressure needed to displace oil in the oil-wet pores. As a consequence, water invaded into more oil-filled pores and increased recovery at the later stages of the LSWF.

ACKNOWLEDGEMENTS

We gratefully acknowledge financial support of Hess Corporation and the School of Energy Resources at the University of Wyoming.

REFERENCES

1. Carll J. F., "The geology of the oil regions of Warren, Venango, Clarion and Butler Counties", Report III, Harrisburg, Pennsylvania, 1880.
2. Yildiz, H. O., Valat, M., and Morrow, N. R., "Effect of brine composition on wettability and oil recovery of a Prudhoe Bay crude oil", *Journal of Canadian Petroleum Technology,* (1999), 38, 01.
3. Tang, G. Q., and Morrow, N. R., "Salinity, temperature, oil composition, and oil recovery by waterflooding", *SPE Reservoir Engineering,* (1997), 12, 04, 269-276.
4. Morrow, N. R., and Buckley, J., "Improved oil recovery by low-salinity waterflooding", *Journal of Petroleum Technology*, (2011), 63, 05, 106-112.
5. Lager, A., et al., "Low salinity oil recovery - An experimental investigation", *Petrophysics,* (2008), 49, 01.
6. Fathi, S. J., Austad, T., and Strand, S., "Water-based enhanced oil recovery (EOR) by "smart water": Optimal ionic composition for EOR in carbonates", *Energy & Fuels*, (2011), 25, 11, 5173-5179.
7. Jerauld, G. R., et al., "Modeling low-salinity waterflooding", *SPE Reservoir Evaluation & Engineering,* (2008), 11, 06, 1000-1012.
8. McGuire, P. L., et al., "Low salinity oil recovery: An exciting new EOR opportunity for Alaska's North Slope", SPE Paper 93903 *presented at the SPE Western Regional Meeting*, 30 March-1 April 2005, Irvine, California.
9. Fogden, A., et al., "Mobilization of fine particles during flooding of sandstones and possible relations to enhanced oil recovery", *Energy & Fuels*, (2011), 25, 4, 1605-1616.
10. Austad, T., RezaeiDoust, A., and Puntervold, T., "Chemical mechanism of low salinity water flooding in sandstone reservoirs", SPE Paper 129767 *presented at the SPE Improved Oil Recovery Symposium,* 24-28 April 2010, Tulsa, Oklahoma.

11. Sorbie, K. S., and Collins, I., "A proposed pore-scale mechanism for how low salinity waterflooding works", SPE Paper 129833 *presented at the SPE Improved Oil Recovery Symposium*, 24-28 April 2010, Tulsa, Oklahoma.
12. Lebedeva, E. V., and Fogden. A., "Micro-CT and wettability analysis of oil recovery from sand packs and the effect of waterflood salinity and kaolinite", *Energy & Fuels*, (2011), 25, 12, 5683-5694.
13. Pu, H., et al., "Low-salinity waterflooding and mineral dissolution", SPE Paper 134042 *presented at the Annual Technical Conference and Exhibition*, 19-22 September 2010, Florence, Italy.
14. Alizadeh, A.H., et al., "Multi-scale experimental study of carbonated water injection: An effective process for mobilization and recovery of trapped oil", *Fuel*, (2014), 132, 219-235.
15. Khishvand, M., Akbarabadi, M., and Piri, M., "Micro-scale experimental investigation of the effect of flow rate on trapping in sandstone and carbonate rock samples", *Advances in Water Resources*, (2016), in press.
16. Khishvand, M., Alizadeh, A.H., and Piri, M., "In-situ characterization of wettability and pore-scale displacements during two- and three-phase flow in natural porous media", *Advances in Water Resources*, (2016), under revision.
17. Alizadeh, A.H., and Piri, M., "The effect of saturation history on three-phase relative permeability: An experimental study", *Water Resources Research*, (2014), 50, 1636-64.
18. Morrow, N. R., "Interfacial phenomena in petroleum recovery", *Surfactant Science Series*, V26, CRC Press, 1990.
19. Kestin, J., Khalifa, H. E., and Correia, R. J., "Tables of the dynamic and kinematic viscosity of aqueous NaCl solutions in the temperature range 20-150°C and the pressure range 0.1-35 MPa", *Journal of physical and chemical reference data*, (1981), 10, 1, 71-88.
20. Amin, R., and Smith, T. N., "Interfacial tension and spreading coefficient under reservoir conditions", *Fluid phase equilibria*, (1998), 142, 1, 231-241.

Table 1- Geometrical and petrophysical properties of the rock samples used in this study.

Sample	Experiment	D & L (mm)	Porosity (%)	Air permeability (mD)
A	LSWF	4.6 & 52	28.32	-
B	HSWF	4.64 & 51	28.97	-
C	Dean-Stark	25.4 & 80	28.37	165
D	XRD analysis	End trim	-	-

Table 2- Physical properties of the fluids used in this study.

Fluid	Experiment	Viscosity at 60°C and 1000 psi (cP)	Density at ambient condition (g/cc)
Low-salinity brine	LSWF	0.3664*	0.999
High-salinity brine	HSWF	0.3836*	1.029
Crude oil	HSWF and LSWF	3.48	0.857

*Estimated from data available in the literature [18-20].

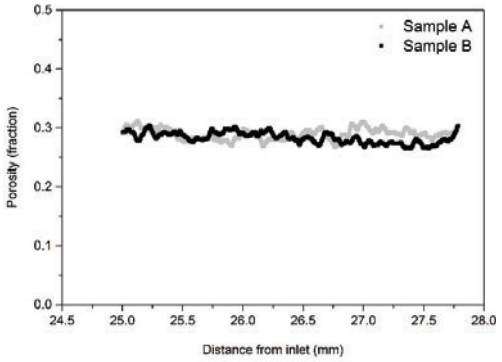

Figure 1 - Porosity distributions along the length of Samples A and B obtained using micro-CT images.

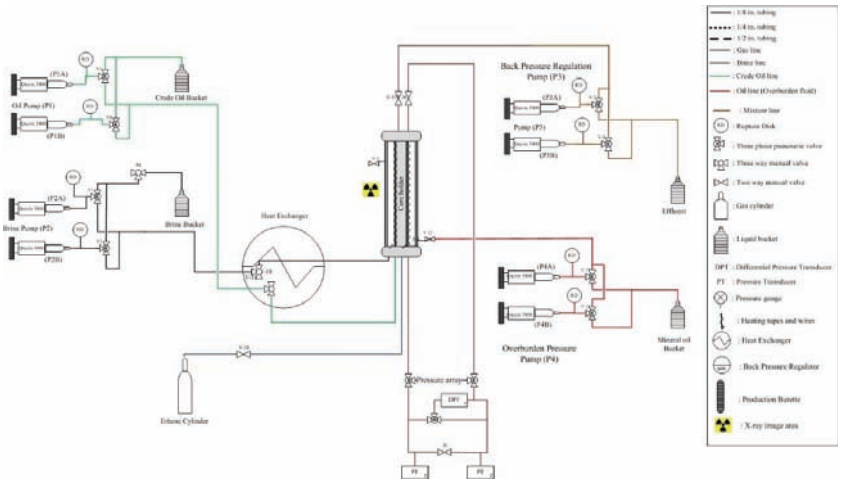

Figure 2 - A schematic diagram of the core-flooding apparatus used in this study.

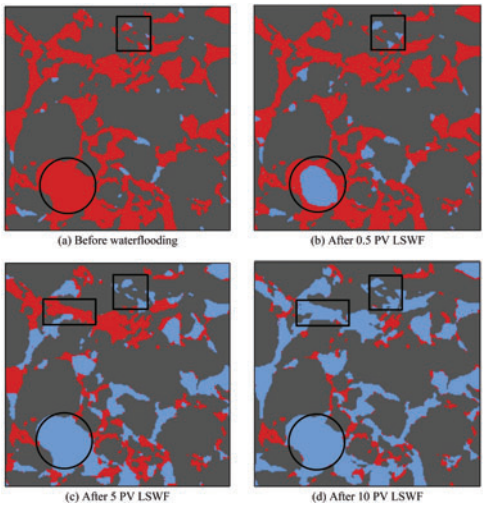

Figure 3 - Visualization of pore-scale fluid occupancies generated at different stages of LSWF experiment (resolution = 1.64 μm; blue: water, red: oil, and gray: solid).

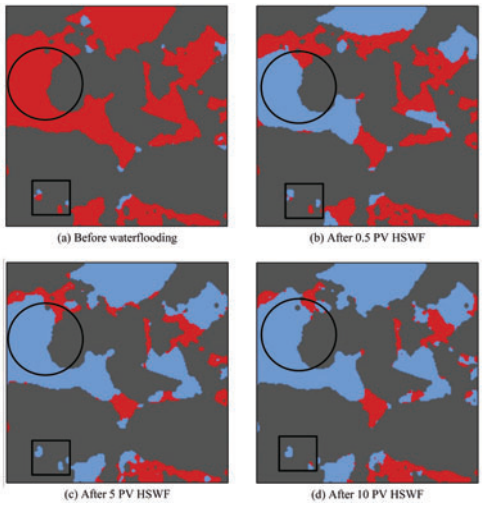

Figure 4 - Visualization of pore-scale fluid occupancies generated at different stages of HSWF experiment (resolution = 1.64 μm; blue: water, red: oil, and gray: solid).

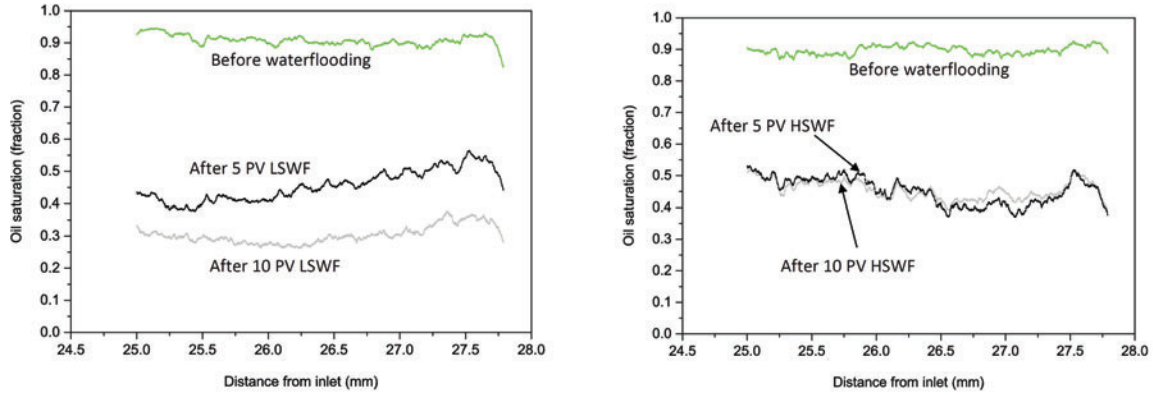

Figure 5 - Oil saturation distributions along the FOV at different stages of LSWF (left) and HSWF (right) tests.

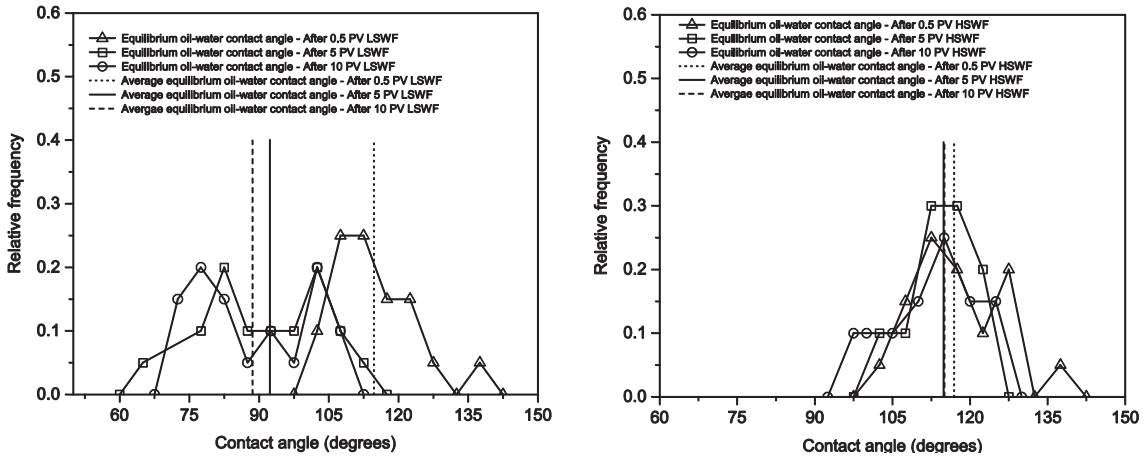

Figure 6 - Histograms of in-situ contact angle distributions during different stages of LSWF (left) and HSWF (right) tests.

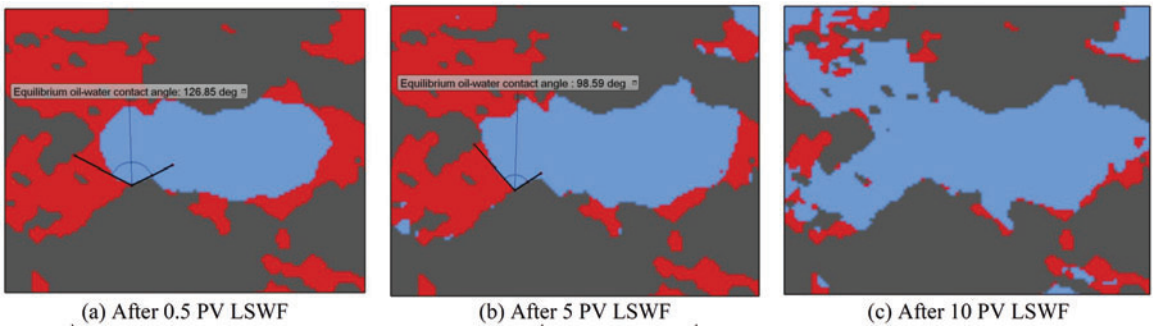

Figure 7 - Two-dimensional cross-sectional views of pore-scale fluid occupancy during primary LSWF test performed on a preserved reservoir sandstone sample (resolution = 1.64 μm; blue: water, red: oil, and gray: solid). The images show changes in wettability during the LSWF and the subsequent invasion of water into an oil-filled pore.